SAND2019-3000C

Electron Transport Algorithms in the Integrated TIGER Series (ITS) Codes

Brian C. Franke and Ronald P. Kensek

Sandia National Laboratories, Albuquerque, NM 87185, bcfrank@sandia.gov, rpkense@sandia.gov

INTRODUCTION

We describe the three electron-transport algorithms implemented in the ITS Monte Carlo codes[1]. The condensed-history method is largely based on the algorithm adapted from the ETRAN code[2, 3]. A hybrid multigroup/continuous-energy method [4] was implemented based on multigroup cross-section data. Recently, a single-scatter analog method was implemented based on the LLNL Evaluated Data Libraries (EDL)[5, 6, 7].

While the underlying cross-section data is similar, each method uses a fundamentally unique method, which at a high level are best characterized as condensed history, multigroup, and single scatter. We discuss the algorithms and present comparisons with experimental data.

ELECTRON TRANSPORT ALGORITHMS

All three methods use similar data. For elastic angular scattering, a high-energy factorization is used for a screened Mott representation while fits to the Riley distributions are used between 1-256 keV. For the condensed-history and multigroup, the high-energy factorization is used above 256 keV using Seltzer's modified screening parameter to help the transition. The analog uses the factorization above 10 MeV with a logarithmic cubic spline to fill the gap for the total elastic cross section relies on user-implemented interpolation of the angular data.

All three methods use the same bremsstrahlung production and spectra cross sections. The condensed-history uses bremsstrahlung angular distributions from Bethe-Heitler theory, while a simpler model is used for the multigroup and analog. The relaxation cascades are similar for the multigroup and condensed history. The analog method uses a complete set of subshell data for relaxation. Each of the three has a different energy-loss model and differ in the treatment of both large and small energy-loss interactions.

Condensed History

The condensed-history method is based on pre-computed energy-loss and angular-scattering distributions. The tracking of the electron is separated into "steps" and "substeps." At the start of the step, the collisional energy loss is sampled from a straggling distribution. Except when encountering a material boundary, the electron is moved a pre-determined substep distance, which depends on the energy of the electron at the start of the step and the resident material. For each substep, the electron is moved straight-ahead and an angular scatter is applied at the end of the substep. Secondary production of knock-on electrons, bremsstrahlung photons, and relaxation radiation is applied after the completion of each substep at randomly assigned locations along the substep.

Angular scattering is computed over a substep centered in the middle of a step using the Goudsmit-Saunderson infinite-medium expansion. Angular deflections due to inelastic-scattering interactions are accounted for approximately by adjusting the elastic-scattering distribution using a $(Z + 1)/Z$ correction. Energy loss is sampled over a step from the Blunck-Leisegang distribution with a correction by Seltzer.

The Jordan-Mack algorithm is used for boundary crossings[8]. An electron substep that intersects a material boundary is truncated at the boundary. An alternative angular-deflection distribution is applied that combines a Gaussian approximation for small angular deflections and samples an appropriate number of large angular deflections from the screened Rutherford distribution.

Bremsstrahlung photon production, knock-on electron production, and electro-ionization events are sampled over each substep. The energy of the sampled bremsstrahlung photons is deducted from the electron. Knock-on electrons due to electro-ionization inelastic scattering are sampled from the Møller distribution and are not correlated to energy loss of the primary electron. Likewise, electro-ionization events are sampled that produce relaxation radiation but are not correlated to the primary electron energy loss or to the production of knock-on electrons. The relaxation cascade for each element accounts for the K-shell, L-shells, an average binding-energy M-shell, and an average binding-energy N-shell.

Hybrid Multigroup/Continuous-Energy

The multigroup-based transport uses cross-section data calculated by the CEPXS code[9]. The physics models in CEPXS were largely based on those that had been implemented in ITS. The CEPXS code integrates the cross section over each energy group or in the case of energy-loss cross sections integrates over both the energy group scattered from and the energy group scattered to. CEPXS also integrates angular scattering moments for each cross section. The angular moments and group-to-group cross sections are summed across all interaction types. The multigroup ITS code does not distinguish between the types of physical interactions and does not preserve correlations, only statistical averages.

CEPXS calculates angular scattering moments, which are converted to discrete scattering angles by a generalized Gauss-quadrature approach, which preserves the total interaction cross section and a selected number of angular scattering moments. This is applied to all group-to-group and within-group scattering, and thus for electrons applies to inelastic scattering, elastic scattering, and bremsstrahlung photon production. The discrete scattering angles can lead to artifacts in the simulation results. A separate treatment is allowed for isotropic angular distribution of particles, such as in the production of Auger electrons, fluorescence photons, or annihilation photons.

There are two unique treatments in the case of electron

Sandia National Laboratories is a multimission laboratory managed and operated by National Technology & Engineering Solutions of Sandia, LLC, a wholly owned subsidiary of Honeywell International Inc., for the U.S. Department of Energy's National Nuclear Security Administration under contract DE-NA0003525.

elastic scattering. A Fokker-Planck approximation is applied, and the total elastic interaction cross section is deliberately not preserved within the simulation. A Gauss-Radau quadrature is used, which includes the scattering cosine of $\mu_0 = 1$ corresponding to no angular deflection.

The Møller distribution is used for large inelastic energy losses and knock-on production above the cutoff energy. A restricted stopping power accounts for soft energy losses, calculated as the difference between the ICRU stopping power and the large energy losses accounted for in group-to-group scattering. The restricted stopping power is treated as piecewise constant in each group, and the continuous-slowing-down approximation (CSDA) is used.

Bremsstrahlung cross sections are evaluated for the photon production, photon angular distribution, and corresponding electron energy loss. Cross sections are also evaluated for the impact ionization that produces relaxation radiation in the form of fluorescence photons and Auger electrons.

Single Scattering

The analog transport is based on the LLNL EDL. The EDL data is represented in tabulated forms with mostly prescribed interpolation schemes. Two notable features of the EDL are extension of cross section data below 1 keV and inclusion of the full set of ionization and relaxation data.

Four types of cross sections are included in the Evaluated Electron Data Library (EEDL): ionization, elastic scatter, bremsstrahlung, and excitation. In all cases, data is tabulated as a function of the incident electron energy, with different energy grids used for each set of data. For each interaction type, the total interaction cross section is included. The ionization data includes the cross section for each subshell and the electron energy-loss distribution for each subshell. The elastic-scattering data includes angular distributions: isotropic at 10 eV, based on fits to the Riley data from 1-256 keV, and based on a high-energy factorization for a screened Mott representation at selected energies of 10 MeV and above. The bremsstrahlung data includes the photon energy spectra and average electron energy-loss per interaction. The excitation data includes only the average energy loss per interaction.

In some cases, we have implemented models that supplement the data. For elastic scattering, it is prescribed that small angle scattering is to be modeled using the screened Rutherford distribution. For electron ionization, we include angular deflections based on particle kinematics. For bremsstrahlung, we have implemented the photon angular distribution that is also used in CEPXS and the ITS "simple-brems" model. We correlate the energy of the bremsstrahlung photon with the energy loss of the incident electron.

We attempt to maintain particle correlations in our implementation. For example, in electro-ionization, the energy loss of the incident electron is the sum of the binding energy of the ionized shell and the secondary knock-on electron, and the ionized shell is relaxed consistent with the EADL.

RESULTS

In this section we compare numerical results using the three electron transport algorithms against experimental results. We generally achieved a relative statistical uncertainty less than 2.5%.

Lockwood Albedo

In Fig. 1, we show the experimental results for the Lockwood electron charge-deposition data in uranium[10]. In Figs. 2-4, we compare all three algorithms against the data. Analog results show issues above 256 keV. We attribute this to the need to interpolate the elastic angular-scattering data between distributions at 256 keV and 10 MeV. Otherwise, there is consistency in the trends of the comparison of the computational results to the experimental results. The condensed-history results are consistently higher than the multigroup

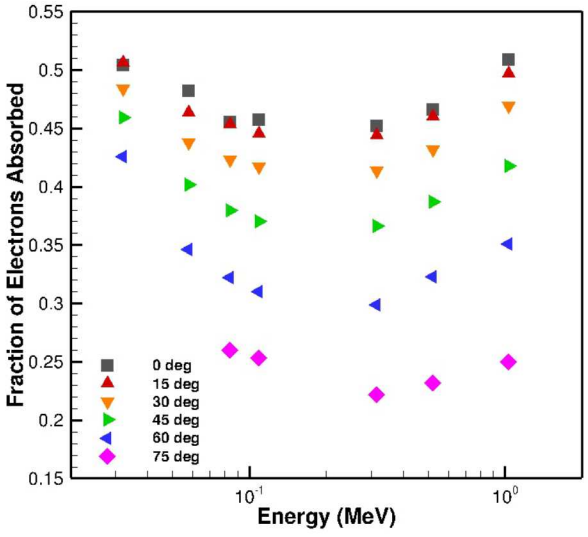

Fig. 1. Lockwood electron deposition experimental results.

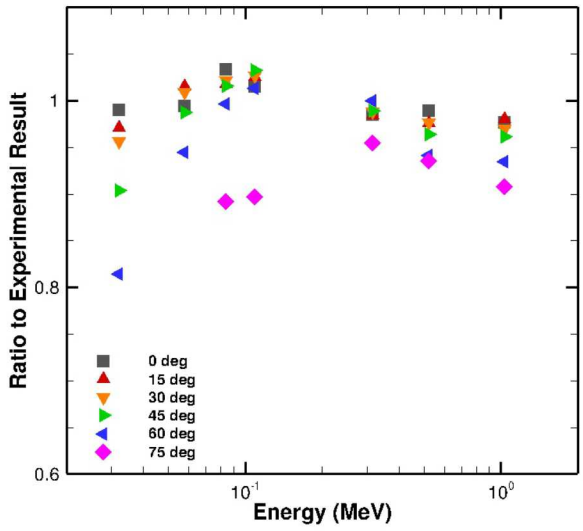

Fig. 2. Ratio of ITS condensed history to experiment.

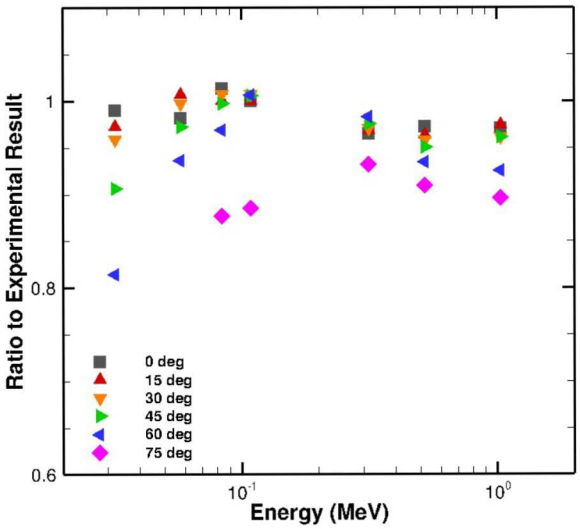

Fig. 3. Ratio of ITS multigroup to experiment.

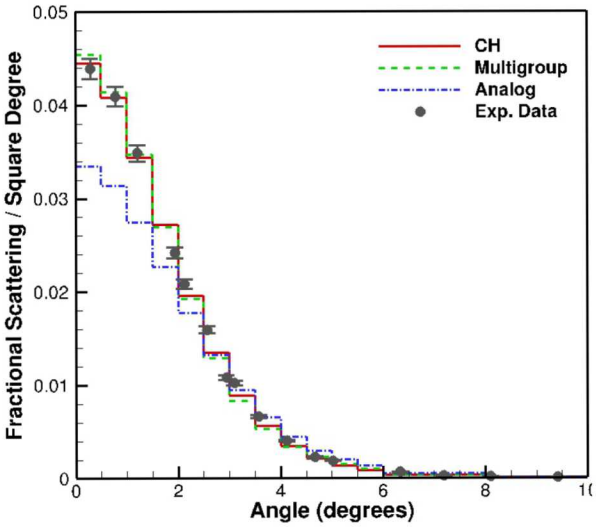

Fig. 5. Electron transmission distribution through a gold foil.

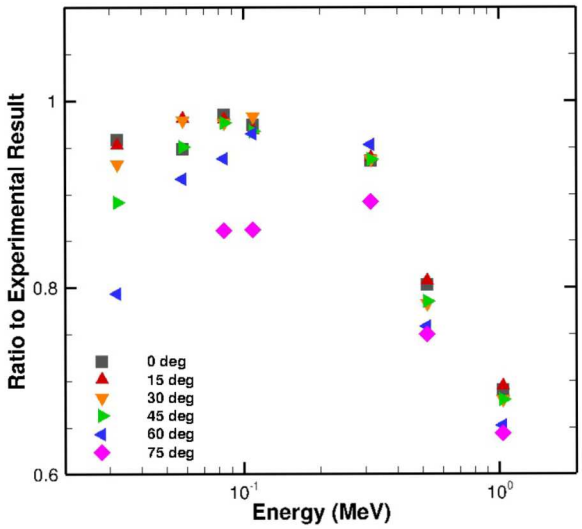

Fig. 4. Ratio of ITS analog to experiment.

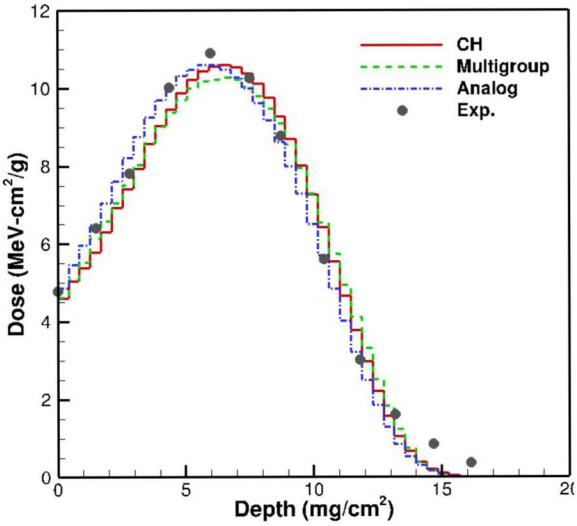

Fig. 6. Energy deposition versus depth in polystyrene.

results. The multigroup results are consistently higher than the analog results. It is known that the condensed-history algorithm systematically underestimates electron reflection due to the straight-ahead substep mechanics.

Hanson Angular Scattering

In Fig. 5, we compare against the experimental measurements of Hanson[11] for the angular distribution of normally incident 15.7 MeV electrons transmitted through a gold foil with a thickness of 9.658 μm. The condensed-history results are in very good agreement with the experimental data. It is worth noting that the foil thickness is less than a substep, therefore all primary electrons are moved directly across the foil, and the boundary-crossing logic is used to evaluate the angular distribution. The multigroup is also in good agreement, but required non-default settings in the cross-section generation to achieve this accuracy. The analog results underestimate the electron transmission at small angular deflections.

McLaughlin Energy Deposition in Polystyrene

Fig. 6 compares numerical results against experimental data[12] for a 100 keV electron beam normally incident on polystyrene. The statistical uncertainty on the Monte Carlo results was less than 2.5% up to a depth of 15 mg/cm^2. Here we see good agreement among all of the methods and the data. There is disagreement with the experimental results beyond about 14 mg/cm^2, but all of the calculations are in close agreement.

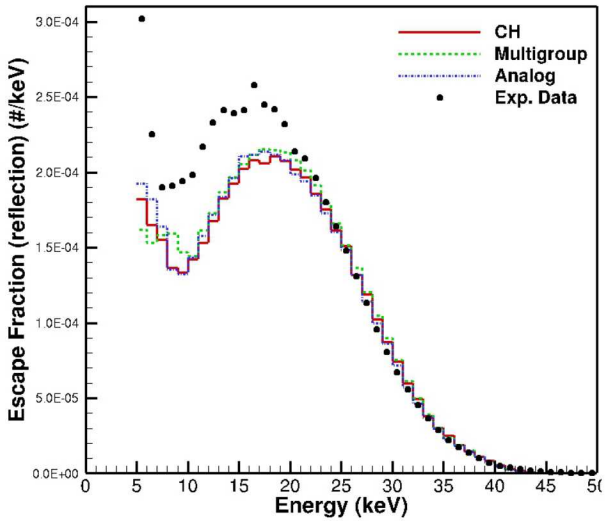

Fig. 7. Reflected electron photo-emission from tantalum.

Dolan Photoemission

Comparison with the Dolan experimental data for reverse photoemission from tantalum[13] is shown in Fig. 7. In this experiment a bremsstrahlung spectrum of source photons was incident on a slab of tantalum and the energy spectrum of electron emission was measured from the incident surface. All of the numerical results below 33 keV have a relative statistical uncertainty less than 1.5%. The calculations are in good agreement with each other above 10 keV, but differ from the experimental results below about 20 keV. Below 10 keV, there are a large number of Auger and fluoresence energies from the L-shells of tantalum, so differences in the relaxation data likely account for the differences in the calculations.

CONCLUSIONS

We have provided a description of the electron-transport algorithms in the Integrated TIGER Series (ITS) codes. Comparisons have been made between the computational results of these algorithms and a variety of experimental data. In general, we observe good agreement between the condensed-history results and the experimental data. The multigroup algorithm can also provide good agreement with the experimental data, though it sometimes required using cross-section generation parameters different from the default settings. For electron sources below 256 keV, we found good agreement between the analog results and experimental results.

ACKNOWLEDGMENTS

Sandia National Laboratories is a multimission laboratory managed and operated by National Technology and Engineering Solutions of Sandia, LLC., a wholly owned subsidiary of Honeywell International, Inc., for the U.S. Department of Energy's National Nuclear Security Administration under contract DE-NA-0003525. This paper describes objective technical results and analysis. Any subjective views or opinions that might be expressed in the paper do not necessarily represent the views of the U.S. Department of Energy or the United States Government.

REFERENCES

1. B. C. FRANKE, R. P. KENSEK, T. W. LAUB, and M. J. CRAWFORD, "ITS Version 6: The Integrated TIGER Series of Coupled Electron/Photon Monte Carlo Transport Codes, Revision 5," Tech. Rep. SAND2008-3331, Sandia National Laboratories (2013).
2. T. M. JENKINS, W. R. NELSON, and A. RINDI, editors, *Monte Carlo transport of electrons and photons*, Ettore Majorana international science series: Physical sciences, Plenum Press, New York (1988).
3. S. SELTZER, "Electron-Photon Monte Carlo Calculations: The ETRAN Code," *Appl. Radiat. Isot.*, **42**, *10*, 917–941 (1991).
4. J. E. MOREL, L. J. LORENCE, R. P. KENSEK, J. A. HALBLEIB, and D. P. SLOAN, "A Hybrid Multigroup/Continuous-Energy Monte Carlo Method for Solving the Boltzmann-Fokker-Planck Equation," *Nucl. Sci. Eng.*, **124**, 369–389 (1996).
5. S. PERKINS, D. CULLEN, and S. SELTZER, "Tables and Graphs of Electron-Interaction Cross Sections from 10 eV to 100 GeV Derived from the LLNL Evaluated Electron Data Library (EEDL), Z=1,100," Tech. Rep. UCRL-50400 Vol 31, LLNL (1991).
6. D. CULLEN ET AL., "Tables and Graphs of Photon-Interaction Cross Sections from 10 eV to 100 GeV Derived from the LLNL Evaluated Photon Data Library (EPDL)," Tech. Rep. UCRL-50400 Vol 6, LLNL (1989).
7. S. PERKINS ET AL., "Tables and Graphs of Atomic Subshell and Relaxation Data Derived from the LLNL Evaluated Atomic Data Library (EADL), Z=1,100," Tech. Rep. UCRL-50400 Vol 30, LLNL (1991).
8. D. JENSEN, *Monte Carlo Calculation of Electron Multiple Scattering in Thin Foils*, Master's thesis, Naval Postgraduate School, Monterey, CA (1988).
9. L. J. LORENCE, JR., J. E. MOREL, and G. D. VALDEZ, "Physics guide to CEPXS: a multigroup coupled electron-photon cross-section generating code," Tech. Rep. SAND89-1685, Sandia National Laboratories (1989).
10. G. J. LOCKWOOD, L. E. RUGGLES, G. H. MILLER, and J. A. HALBLEIB, "Electron energy and charge albedos - calorimetric measurement vs Monte Carlo theory," Tech. Rep. SAND80-1968, Sandia National Laboratories (1981).
11. A. O. HANSON, L. H. LANZL, E. M. LYMAN, and M. B. SCOTT, "Measurement of Multiple Scattering of 15.7-MeV Electrons," *Physical Review*, **84**, *4* (1951).
12. W. L. MCLAUGHLIN and E. K. HUSSMAN, "The Measurement of Electron and Gamma-Ray Dose Distributions in Various Media," in "Large Radiation Sources for Industrial Processes," IAEA-SM-123/43.
13. K. W. DOLAN, "X-ray-Induced Electron Emission from Metals," *J. Appl. Phys.*, **46**, *6*, 2456–2463 (1975).